

How to erase surface plasmon fringes

Aurelien Drezet, Andreas Hohenau, Andrey L. Stepanov, Harald Dittlbacher, Bernhard Steinberger, Nicole Galler, Franz R. Aussenegg, Alfred Leitner, and Joachim R. Krenn

Citation: [Applied Physics Letters](#) **89**, 091117 (2006); doi: 10.1063/1.2339043

View online: <http://dx.doi.org/10.1063/1.2339043>

View Table of Contents: <http://scitation.aip.org/content/aip/journal/apl/89/9?ver=pdfcov>

Published by the [AIP Publishing](#)

Articles you may be interested in

[Plasmon induced transparency in a surface plasmon polariton waveguide with a comb line slot and rectangle cavity](#)

Appl. Phys. Lett. **104**, 231114 (2014); 10.1063/1.4883647

[Direct measurement of versatile surface plasmon polaritons excited by split polarization](#)

Appl. Phys. Lett. **98**, 081107 (2011); 10.1063/1.3552673

[Plasmonic implementation of a quantum eraser for imaging applications](#)

J. Appl. Phys. **108**, 063110 (2010); 10.1063/1.3485810

[Fourier plasmonics: Diffractive focusing of in-plane surface plasmon polariton waves](#)

Appl. Phys. Lett. **91**, 081101 (2007); 10.1063/1.2772756

[Interference in far-field radiation of two contra-propagating surface plasmon polaritons in the Kretschmann configuration](#)

J. Vac. Sci. Technol. A **16**, 1420 (1998); 10.1116/1.581161

The image shows the cover of the journal Applied Physics Reviews. It features a blue background with a molecular structure of spheres and sticks. On the left, there is a smaller image of the journal cover showing a diagram of a device. The text 'AIP Applied Physics Reviews' is at the top left. The main title 'NEW Special Topic Sections' is in large white letters. Below it, 'NOW ONLINE' is in yellow, followed by 'Lithium Niobate Properties and Applications: Reviews of Emerging Trends' in white. The AIP logo and 'Applied Physics Reviews' are at the bottom right.

NEW Special Topic Sections

NOW ONLINE
Lithium Niobate Properties and Applications:
Reviews of Emerging Trends

AIP Applied Physics Reviews

How to erase surface plasmon fringes

Aurelien Drezet,^{a)} Andreas Hohenau, Andrey L. Stepanov, Harald Dittlbacher, Bernhard Steinberger, Nicole Galler, Franz R. Aussenegg, Alfred Leitner, and Joachim R. Krenn

Institute of Physics, Karl-Franzens-University, Universitätsplatz 5, 8010 Graz, Austria and Erwin Schrödinger Institute for Nanoscale Research, Karl-Franzens-University, Universitätsplatz 5, 8010 Graz, Austria

(Received 23 June 2006; accepted 9 July 2006; published online 31 August 2006)

The authors report on the imaging of surface plasmon polaritons (SPPs) by leakage radiation microscopy in both direct and Fourier space. They show that manipulating the intensity distribution in the Fourier plane allows them to selectively image SPP beams propagating along specific directions. Thereby individual SPP beams are made accessible for direct quantitative analysis which is important in cases where the interaction between different SPP beams leads to interference fringes obscuring the individual components. © 2006 American Institute of Physics.

[DOI: 10.1063/1.2339043]

The miniaturization of conventional optical elements and devices into nanoscale dimensions is restricted by diffraction to about half the effective light wavelength. One promising way to overcome this restriction is the use of surface plasmon polaritons (SPPs) instead of light waves. SPPs are quasi-two-dimensional electron excitations propagating along a metal/dielectric interface coupled to electromagnetic fields that decay exponentially into both media defining the interface.¹ As recently demonstrated, besides near field optical microscopy² and fluorescence mapping,³ leakage radiation microscopy (LRM) is a powerful technique for SPP imaging.^{4–6} It was shown that LRM allows for quantitative measurements of the spatial SPP field profile and thus for the measurement of quantities as SPP reflection, transmission, and scattering efficiencies.^{6,7} Besides imaging in direct space, LRM can as well be applied in Fourier space, i.e., the SPP wave vector space.^{4,8–11} Here, we report on LRM operated simultaneously in direct and Fourier spaces, with the ability to filter specific SPP wave vector components in the Fourier plane which is the back focal plane of the imaging optics. This approach allows us to selectively image SPP beams propagating into different directions and to erase SPP fringes from the direct space image which result from the interference of these beams. In principle, quantitative measurements on SPP propagation can thus be achieved in spatial regions where due to interference direct measurements by, e.g., conventional LRM or near field scanning microscopy are not possible.

The intensity decay length of a SPP wave in a planar metal thin film between two dielectric media (usually glass and air) defines its intrinsic decay length $L_{\text{SPP}} = 1/2k''_{\text{SPP}}$, k''_{SPP} being the imaginary part of the complex SPP wave vector modulus $k_{\text{SPP}} = k'_{\text{SPP}} + k''_{\text{SPP}}$. Intrinsic losses are caused by Ohmic damping and leakage radiation (LR).¹ LR is emitted into the higher refractive index medium (glass substrate) when SPP fields propagating along the metal/air interface leak through the metal film and reach the substrate. In reversal of the so-called Kretschmann excitation scheme,¹ LR is emitted in a narrow range around a characteristic angle of inclination θ_{LR} with respect to the interface normal. At this

angle the LR wave satisfies $k'_{\text{SPP}} = 2\pi/\lambda_{\text{SPP}} = nk_0 \sin \theta_{\text{LR}}$, where λ_{SPP} is the SPP wavelength, n the refractive index of the glass substrate, and k_0 the modulus of the vacuum light wave vector. The intensity at any point of the image plane in LRM is directly proportional to the SPP intensity at the conjugate point at the metal/air interface, i.e., in the object plane of the microscope.^{6,7}

The experimental LRM setup is sketched in Fig. 1. SPPs at a wavelength of about 785 nm are excited by focusing laser light at a vacuum wavelength $\lambda_0 = 800$ nm through a microscope objective O_1 (50×, numerical aperture of 0.7) onto an electron-beam lithographically fabricated 50 nm high and 200 nm wide gold ridge on a 50 nm thick gold thin

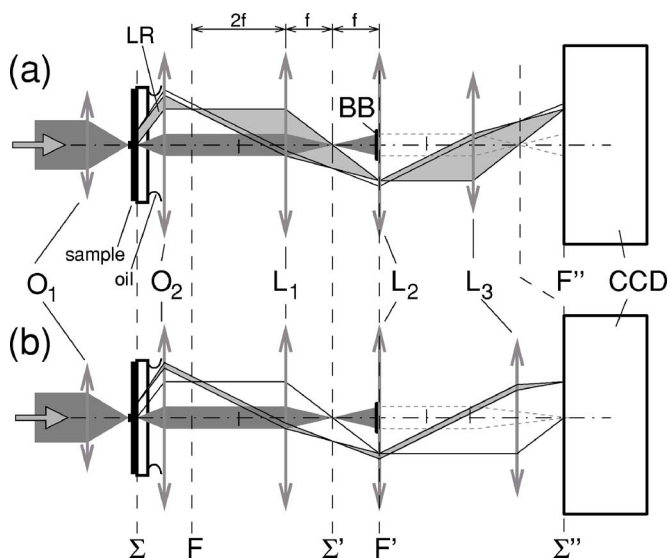


FIG. 1. Experimental scheme for leakage radiation microscopy. SPPs are excited by laser light focused by the microscope objective O_1 (50×, numerical aperture of 0.7) onto a structured gold thin film on a glass substrate. Leakage radiation (LR) emitted into the glass substrate from the gold/glass interface Σ is collected by the immersion microscopy objective O_2 (63×, numerical aperture of 1.25) and imaged by a charge-coupled-device (CCD) camera. Depending on the lateral position of the convex lens L_3 either (a) the back focal plane or (b) the sample plane is imaged (for further details see text). BB beam block, $L_{1,2,3}$ convex lenses, f focal length of L_1 and L_2 ; Σ , Σ' , and Σ'' , sample plane and images thereof; F , F' , and F'' back focal plane and images thereof.

^{a)}Electronic mail: aurelien.drezet@uni-graz.at

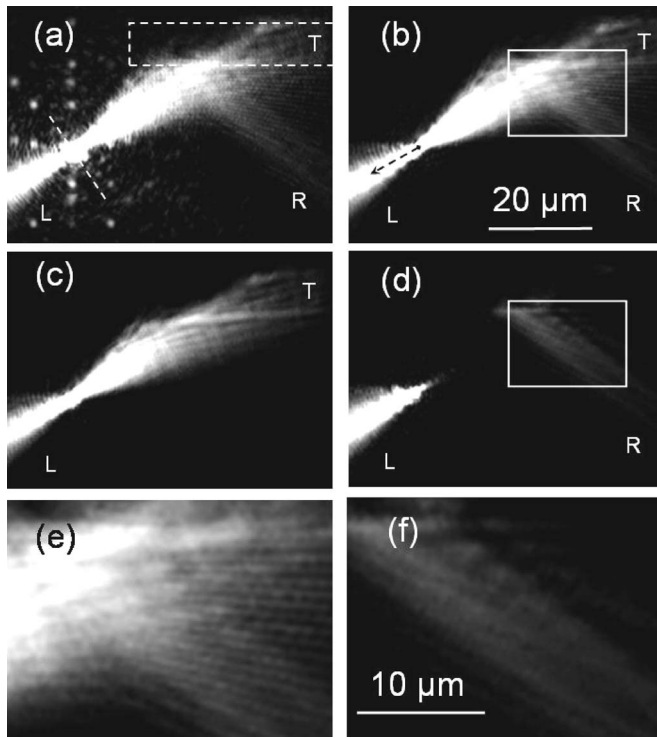


FIG. 2. Direct space LRM imaging of two SPPs beams launched from the ridge and propagating to the lower left (L) and upper right to be partly reflected (R) and transmitted (T) by the Bragg mirror. (a) Image with no beam block. Ridge and Bragg mirror are indicated by the dashed line and rectangle, respectively. (b) Image with central beam block in F' [C , as marked in Fig. 3(a)]. The box indicates the image area of (e). (c) Image with beam blocks for C and R , as marked in Fig. 3(a). (d) Image with beam blocks for C and T , as marked in Fig. 3(a). The box indicates the image area of (f). (e) and (f) magnified areas from (b) and (d), respectively.

film. The gold film is deposited on a $150\text{ }\mu\text{m}$ thick glass substrate. LR from the sample plane Σ is collected by an oil immersion objective O_2 ($63\times$, numerical aperture of 1.25). In addition, the back focal plane F which is contained within O_2 is projected with the lens L_1 into the plane F' where the light intensity distribution can be selectively blocked. Finally, we use two auxiliary convex lenses L_2 (located in F') and L_3 for imaging either the object plane or the back focal plane (depending on the position of L_3) onto a charge-coupled-device (CCD) camera [F'' , Fig. 1(a) and Σ'' , Fig. 1(b), respectively].

Figure 2(a) shows a direct space LRM image of the two SPP beams excited by focusing the laser onto the gold ridge which is marked by the dashed line.¹² As reported before the image is obscured due to laser light transmitted directly through the gold film, leading to strong overexposure at the laser focus position and a CCD related artifact forming a pattern of bright spots.^{6,7} Clearly, the respective contributions from the incident laser beam and the LR cannot be separated in the sample plane image. However, one can do so in the the back focal plane F of the immersion objective which is the Fourier plane with respect to the sample plane and thus a map of the two-dimensional momentum distribution of the light emitted in Σ . The signals corresponding to the two SPP beams propagating to the lower left and upper right in Fig. 2(a) are therefore confined to the circumference of a circle with radius $|k'_{\text{SPP}}|$, as marked by the letters L and T respectively, in Fig. 3(a). In contrast, the directly transmitted beam is located around the center of this circle [C in Fig.

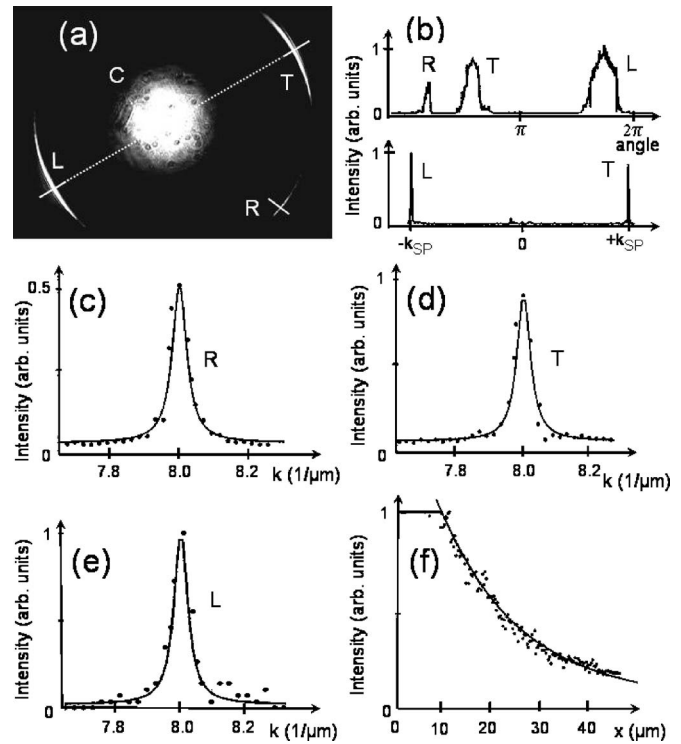


FIG. 3. Fourier plane LRM imaging. (a) Image corresponding to Fig. 2(a). The letters indicate the wave vector components of the directly transmitted laser beam (C) and the SPP beams propagating to the lower left (L), to the upper right including the components transmitted by the Bragg mirror (T), and being reflected by the Bragg mirror (R). To acquire the images in Fig. 2 the respective areas have been completely blocked. (b) Cross cuts along the circumference of the ring with radius $|k'_{\text{SPP}}|$ in counterclockwise direction (upper panel) and along the dashed line in (a) (lower panel) with, however, the central laser spot removed. [(c)–(e)] Cross cuts along the short solid lines in (a) (symbols) and respective fits (solid curves). In all graphs [(b)–(e)] the intensity is normalized by setting the maximum intensity of L to 1. (f) Direct space cross cut along the dashed line in Fig. 2(b) (symbols) and respective fit (solid line).

3(a)]. Further features in these images will be discussed below. By introducing a central beam block in the plane F' (Fig. 1) it is now possible to eliminate the direct contribution of the laser beam to the LRM images. The effect of the central beam block is evident from the direct space image in Fig. 2(b) where no more artifact and overexposure close to the SPP launch ridge are present, as compared to Fig. 2(a).

The SPP beam propagating to the upper right in Figs. 2(a) and 2(b) impinges on a Bragg mirror with a grating constant of 555 nm constituted by gold ridges 50 nm high and 140 nm wide. The mirror area is indicated by the dashed box in Fig. 2(a). While this mirror is designed for an angle of incidence of 45° , we use here an angle of 65° which gives rise to reflected and transmitted SPP beams (R and T , respectively) of roughly equal intensity. As expected, the area where incident and reflected SPP beams overlap [box in Fig. 2(b)] is dominated by interference fringes.

For further analysis we turn back to the Fourier plane image in Fig. 3(a). An angular cross cut along the circle with radius $|k_{\text{SPP}}|$ and a radial cross cut along the dotted line L - T are plotted in Fig. 3(b). In the former the three SPP beams are clearly displayed with their respective intensities and angular widths. The latter shows two peaks with a width that is a direct measure of the SPP damping. As outlined in Ref. 13 the peaks are expected to have a Lorentzian shape with a full width at half maximum equal to $2k'_{\text{SPP}}$. Indeed, as

shown in Figs. 3(c)–3(e) all peaks corresponding to the SPP beams L , T , and R are very well described by Lorentzian curves with a damping value $k''_{\text{SPP}} = 0.0251 \mu\text{m}^{-1}$ as the single fit parameter. This value is in agreement with the value deduced from literature data on the optical properties of gold for the used wavelength.¹⁴ In addition we plot in Fig. 3(f) the SPP decay in real space along the direction defined by the dashed arrow in Fig. 2(b).¹⁵ The experimental data are well fit by an exponential decay defined by $L_{\text{SPP}} = 20.0 \mu\text{m}$ which is almost perfectly consistent with $L_{\text{SPP}} = 1/2k''_{\text{SPP}}$ deduced before.

To extend our control over the SPP wave vector distribution in the LRM imaging process we now add off-axis beam blocks in F' to the C beam block. By blocking the area marked R in Fig. 3(a) we eliminate the reflected beam from the direct space image as seen in Fig. 2(c). On the other hand, blocking T allows us to remove the transmitted SPP beam (together with the whole SPP beam propagating to the upper right from the ridge) as shown in Fig. 2(d). Most importantly, however, is the fact that together with the suppression of an individual SPP beam from the direct space image interference fringes due to the interaction of this SPP beam with another one are erased as well. As already mentioned above, the area close to the Bragg mirror in Fig. 2(b) is dominated by fringes due to interference of the SPP beam incident on the Bragg mirror and the reflected SPP beam R . A magnified view of this area as enclosed by the box in Fig. 2(b) is shown in Fig. 2(e). The corresponding magnified image from Fig. 2(d) where C and T are blocked in F' is shown in Fig. 2(f). Obviously the fringes dominating Fig. 2(e) are absent from this image and the isolated SPP beam R is recovered and thus directly accessible for quantitative analysis.

In summary, LRM proves to be a straightforward and reliable technique for probing SPP fields in direct and Fourier spaces. We have shown that controlling the Fourier plane intensity distribution allows us to selectively erase SPP beams and interference fringes, thereby isolating SPP beams for individual analysis.

The authors acknowledge financial support from the EU under Project Nos. FP6 NMP4-CT-2003-505699 and FP6 2002-IST-1-507879 and the Lisa Meitner programm of the Austrian Science Foundation (M868-N08).

- ¹H. Raether, *Surface Plasmons*, Springer Tracts in Modern Physics Vol. 111, edited by G. Höhler (Springer, Berlin, 1988).
- ²J. C. Weeber, J. R. Krenn, A. Dereux, B. Lamprecht, Y. Lacroute, and J. P. Goudonnet, *Phys. Rev. B* **64**, 045411 (2001).
- ³H. Ditlbacher, J. R. Krenn, G. Schider, A. Leitner, and F. R. Aussenegg, *Appl. Phys. Lett.* **81**, 1762 (2002).
- ⁴B. Hecht, H. Bielefeldt, L. Novotny, Y. Inouye, and D. W. Pohl, *Phys. Rev. Lett.* **77**, 1889 (1996).
- ⁵A. Bouhelier, T. Huser, H. Tamaru, H.-J. Güntherodt, D. W. Pohl, F. I. Baida, and D. Van Labeke, *Phys. Rev. B* **63**, 155404 (2001).
- ⁶A. Stepanov, J. R. Krenn, H. Ditlbacher, A. Hohenau, A. Drezet, B. Steinberger, A. Leitner, and F. R. Aussenegg, *Opt. Lett.* **30**, 1524 (2005).
- ⁷A. Drezet, A. L. Stepanov, H. Ditlbacher, A. Hohenau, B. Steinberger, F. R. Aussenegg, A. Leitner, and J. R. Krenn, *Appl. Phys. Lett.* **86**, 074104 (2005).
- ⁸H. Simon and J. K. Guha, *Opt. Commun.* **18**, 391 (1976).
- ⁹T. Y. N. Fang, Z. Liu, and X. Zhang, *Opt. Express* **11**, 682 (2003).
- ¹⁰H. K. D. Nomura and H. Shibuya, *Appl. Opt.* **43**, 2409 (2004).
- ¹¹A. Giannattasio and W. L. Barnes, *Opt. Express* **13**, 428 (2005).
- ¹²H. Ditlbacher, J. R. Krenn, N. Felidj, B. Lamprecht, G. Schider, M. Salerno, A. Leitner, and F. R. Aussenegg, *Appl. Phys. Lett.* **80**, 404 (2002).
- ¹³J. J. Burke, G. I. Stegeman, and T. Tamir, *Phys. Rev. B* **33**, 5186 (1986).
- ¹⁴P. B. Johnson and R. W. Christy, *Phys. Rev. B* **6**, 4370 (1972).
- ¹⁵A. Drezet, A. L. Stepanov, A. Hohenau, B. Steinberger, N. Galler, H. Ditlbacher, A. Leitner, F. R. Aussenegg, J. R. Krenn, M. U. Gonzalez, and J. C. Weeber, *Europhys. Lett.* **74**, 693 (2006).